Chemical Science

ROYAL SOCIETY OF CHEMISTRY

EDGE ARTICLE

View Article Online
View Journal | View Issue

Check for updates

Cite this: *Chem. Sci.*, 2021, **12**, 2071

All publication charges for this article have been paid for by the Royal Society of Chemistry

Received 26th October 2020
Accepted 15th December 2020

DOI: 10.1039/d0sc05885h

rsc.li/chemical-science

Designing tubular conducting polymer actuators for wireless electropumping†

Bhavana Gupta,‡[ab] Lin Zhang,‡[ab] Ambrose Ashwin Melvin,[a] Bertrand Goudeau,[a] Laurent Bouffier [a] and Alexander Kuhn *[a]

Rational design and shaping of soft smart materials offer potential applications that cannot be addressed with rigid systems. In particular, electroresponsive elastic materials are well-suited for developing original active devices, such as pumps and actuators. However, applying the electric stimulus requires usually a physical connection between the active part and a power supply. Here we report about the design of an electromechanical system based on conducting polymers, enabling the actuation of a wireless microfluidic pump. Using the electric field-induced asymmetric polarization of miniaturized polypyrrole tubes, it is possible to trigger simultaneously site-specific chemical reactions, leading to shrinking and swelling in aqueous solution without any physical connection to a power source. The complementary electrochemical reactions occurring at the opposite extremities of the tube result in a differential change of its diameter. In turn, this electromechanical deformation allows inducing highly controlled fluid dynamics. The performance of such a remotely triggered electrochemically active soft pump can be fine-tuned by optimizing the wall thickness, length and inner diameter of the material. The efficient and fast actuation of the polymer pump opens up new opportunities for actuators in the field of fluidic or microfluidic devices, such as controlled drug release, artificial organs and bioinspired actuators.

Introduction

The concept of wireless stimuli responsive actuators is a promising alternative to avoid the complexity of hard-wired control systems.[1–6] Actuators based on smart materials offer a huge range of promising applications, from grippers to energy conversion, drug delivery, microsurgery and other medical applications.[4,7–10] Out of this large variety of topics, one increasingly interesting field of investigation is the use of chemistry-based actuators for controlling fluid dynamics *e.g. via* valves and pumps made out of stimuli responsive soft materials, analogous to natural systems.[11–14] However, the majority of alternative pumping concepts,[4,15] including those involving actuators using smart materials,[16] requires a physical connection to an external power supply. This eventually limits their application potential, especially in the case of miniaturized systems. Recently, passive and self-powered microfluidic pumping strategies have been developed based on various stimuli responsive materials, driven by different energy sources. However, a precise control of flow rate might be sometimes difficult.[17–19] Autonomous intestine-like motion of a tubular gel was obtained by converting chemical energy into mechanical motion.[17] Light-driven self-regulated flow control has been carried out with different kinds of soft pumps made out of stimuli-responsive hydrogels[14,19] or liquid crystal polymers.[18] Fluid flow has also been reported in carbon nanopipes *via* asymmetric polypyrrole (PPy) deposition at the two extremities by using bipolar electrochemistry.[20] Last but not least, soft pumping systems can be driven with the help of electric fields. However, compared to other types of triggers, the development of electro-driven soft pumps is still limited by the essential requirement of an ohmic contact in order to plug the active soft matter into a power supply.[21,22] Thus, a concept, which might allow driving soft pumps with electricity, but without requiring a physical connection, would greatly improve their applicability and functionality.

Among all classes of soft materials, conducting polymers are probably one of the most advanced examples of soft stimuli-responsive smart matter, due to very versatile features that allow their use as building blocks for the development of soft machines and robots at the interface between biology and engineering.[23,24] Recent potential applications of such polymers are *e.g.* in microelectromechanical systems (MEMS),[25] for biomimetic robotic functions[26,27] as well as in microinjection devices.[16] Until now, soft materials based on conducting polymers have evolved as an interesting ingredient of pumps, however, there is still a strong need for miniaturizable soft pumping systems relying on conducting polymers, which can

[a]*Univ. Bordeaux, ISM, CNRS UMR 5255, Bordeaux INP, ENSCBP, 16 Avenue Pey Berland, 33607 Pessac, France. E-mail: kuhn@enscbp.fr*

[b]*National & Local Joint Engineering Research Center for Applied Technology of Hybrid Nanomaterials, Henan University, Kaifeng 475004, China*

† Electronic supplementary information (ESI) available. See DOI: 10.1039/d0sc05885h

‡ B. Gupta and L. Zhang made equal contribution to the work.

Open Access Article. Published on 15 December 2020. Downloaded on 5/26/2026 11:38:55 AM. This article is licensed under a Creative Commons Attribution-NonCommercial 3.0 Unported Licence.

© 2021 The Author(s). Published by the Royal Society of Chemistry

Open Access Article. Published on 15 December 2020. Downloaded on 5/26/2026 11:38:55 AM.
This article is licensed under a Creative Commons Attribution-NonCommercial 3.0 Unported Licence.

be triggered in a wireless mode in order to be integrated into MEMS and microfluidic devices.

PPy is a landmark conducting polymer, which has been already successfully used for actuation by transforming electric energy into mechanical action and it has been widely explored for various applications.[28,29] For example, actuators with an integrated biofuel cell, providing electric power by the oxidation of glucose in the presence of oxygen, have been reported recently for implantable or ingestible medical devices without any need of batteries.[30] Yang *et al.* demonstrated that microwave radiation allows generating a DC electric field through a rectenna, leading to the wireless actuation of a hybrid PPy device.[31] In most of these systems, only one extremity of the polymer participates in the actuation, while the other end needs to be connected to an electric power supply. This might hamper the integration of such actuators in microdevices. Stimulating simultaneously the deformation of both extremities of the polymer would not only improve the efficiency, but also increase the functionality of the actuator. Wireless actuation of PPy has been recently reported for generating crawling motion,[26,32] as well as the basis for the electromechanical read-out of chemical and biochemical information.[33–35] The key ingredient of this approach is a break of symmetry, induced by bipolar electrochemistry. In this case, two coupled electrochemical reactions occur simultaneously at the two extremities of the polymer object. This typical feature of bipolar electrochemistry has been previously also explored for functional material synthesis,[36–40] surface patterning,[41,42] locomotion,[43,44] sensing[33,45,46] and light emission.[47–49] In the present contribution, we investigate for the first time the possibility of using this versatile concept for the development of wireless tubular electrochemical actuators based on an electric field responsive conducting polymer *i.e.* PPy, leading to a microfluidic pumping device with tunable features and performance.

Results and discussion

The crucial ingredient for all the experiments related to this work is a tubular structure made out of conducting polymer. We adapted a template type synthesis approach to generate the polymer in a homogeneous way around a metal wire, which later can be removed either mechanically or by chemical dissolution. PPy tubes were obtained by galvanostatic electropolymerization as shown in Scheme 1. The electrochemical cell consists of a cylinder-shaped Pt counter electrode (C), an Ag/AgCl reference electrode (R), and a copper wire as working electrode (W). Dodecyl benzenesulfonate (DBS) anions are used as supporting electrolyte in a solution containing pyrrole (Py) monomer. During the synthesis of the polymer tube, the main hurdle is the removal of the final polymer object from the copper wire, which is used as a temporary template. To overcome this technical issue, the copper wire surface is first coated with silver paint as a lubricant, which facilitates the removal of the polymer tube from the copper wire after the electropolymerization process. Once PPy is obtained in its tubular and homogeneous form, as illustrated in the two insets of Scheme 1 (optical and SEM images), it is possible to investigate its properties for wireless electropumping. The pumping efficiency is optimized by varying several parameters such as wall thickness, inner diameter and tube length as described in the following section.

The experimental set-up for bipolar electropumping with a PPy tube is illustrated in Scheme 2. The polymer object acts as a bipolar electrode when it is positioned on an insulating support in the middle of the bipolar electrochemical cell. An electric field is generated by the feeder electrodes, placed 4 cm apart. The electric field induces a polarization of the polymer tube with respect to the surrounding electrolyte solution, generating δ^+ and δ^- poles. At the δ^+ extremity, electrochemical overoxidation of PPy takes place, because the as-synthesized polymer is already in a completely oxidized state after the oxidative electropolymerization process. If this overoxidation is strong enough and extends over a significant fraction of that tube extremity, this part of the bipolar object will become non-conductive, leading to a symmetry break which will allow unidirectional pumping (*vide infra*). On the other hand, the δ^- end of the polymer undergoes electrochemical reduction.

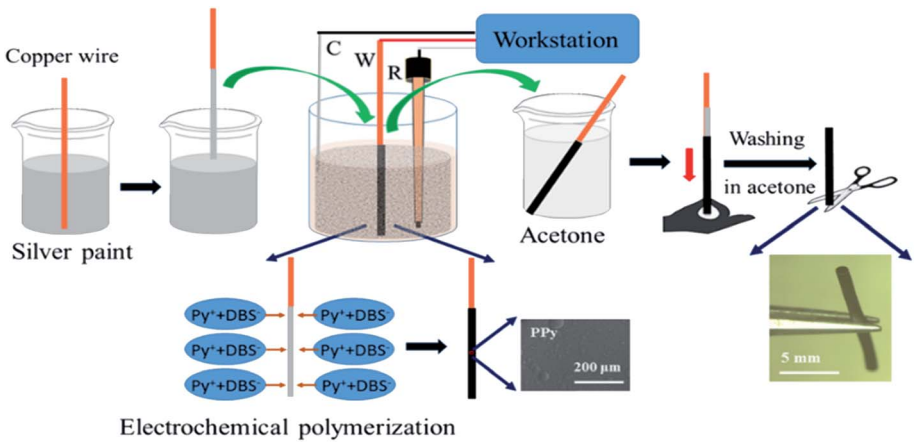

Scheme 1 Synthesis of tubular polypyrrole actuators. C: counter electrode, R: reference electrode and W: working electrode for electrochemical polymerization of pyrrole (Py) to synthesize polypyrrole (PPy) doped with dodecyl benzenesulfonate (DBS) anions. The electron microscopy picture shows the surface of the generated PPy tube. The optical image illustrates the final polymer tube after removal of the template wire.

© 2021 The Author(s). Published by the Royal Society of Chemistry

Open Access Article. Published on 15 December 2020. Downloaded on 5/26/2026 11:38:55 AM.
This article is licensed under a Creative Commons Attribution-NonCommercial 3.0 Unported Licence.

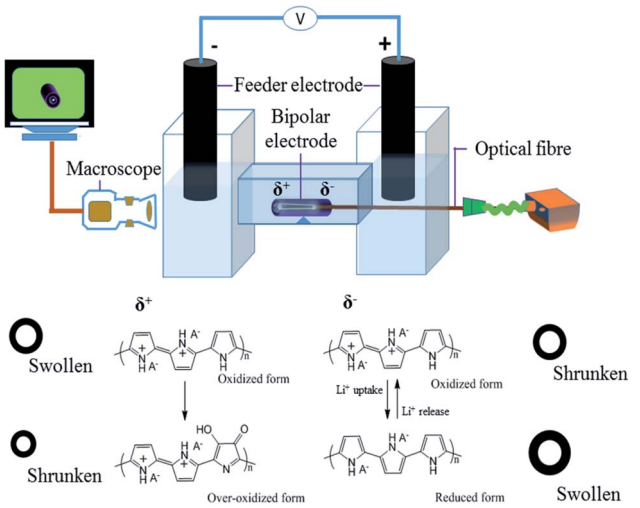

Scheme 2 Schematic illustration of the bipolar electrochemical cell and the mechanism of wireless electropumping, with the associated redox processes occurring at the left and right extremity of the polymer tube (δ^+ and δ^- polarization respectively). The feeder electrodes are graphite rods and the bipolar electrode is the polypyrrole tube. An optical fibre is used for illumination to better visualize the internal space of the tube with a stereo macroscope. The reaction scheme illustrates the processes occurring at the two extremities of the tube during the first polarization cycle when the potential difference is sufficiently high and applied for a long enough time to induce over-oxidation at the δ^+ end, and thus a symmetry break leading to unidirectional pumping.

The dopant used during the electrosynthesis is DBS, which is a rather large molecule due to the presence of the long alkyl side chain featuring twelve carbon atoms.

Thus, during the redox processes, involving the polymer, charge neutrality is maintained by lithium cation exchange.[32,50,51] During the reduction of the polymer, the loss of positive charges in the polymer is equilibrated by an uptake of the positively charged lithium ions. This charge compensation mechanism leads to local swelling (due to insertion of Li^+), or shrinking when the polymer is reoxidized (*i.e.* accompanied by a release of Li^+). *In fine* these local volume changes generate the pumping effect.

The ion exchange at both ends occurs preferentially at the outer tube surface due to its rougher morphology, and thus higher active surface area, generated during the electropolymerization on the template wire. The internal surface is much smoother, because it has been in contact with the wire surface during the growth, analogous to what has been observed in a previous study with flat layers of conducting polymer.[32] This causes an anisotropic swelling at the δ^- end of the polymer tube, accompanied by an increase of its inner diameter. During over-oxidation at the opposite δ^+ extremity, only a slight shrinking effect is observed. Inverting the polarity of the feeder electrodes changes the polarization of the polymer tube. This 'Umpolung' causes now a shrinking effect and a decrease in inner diameter at the δ^+ extremity (which was the δ^- extremity in the previous cycle) accompanied by a swelling at the δ^- extremity (which was the δ^+ extremity in the previous cycle). Due to the over-oxidation during the first bipolar cycle, the degree of swelling and shrinking is not identical at both ends, and therefore the overall system behaves in an asymmetric way, which is the key ingredient for an efficient unidirectional pumping. In order to better observe and characterize the dynamic behaviour of the PPy tube, the inside of the tube was illuminated with an optical fiber during dynamic video recordings. Various characteristics of the polymer tube, as well as other experimental parameters such as solution composition and magnitude of the applied electric field, will influence not only the amplitude of swelling, but also the response time, and thus the pumping efficiency. Since the δ^- extremity during the first bipolar cycle remains electrochemically more active, its behaviour is evaluated in terms of cross sectional area change as a function of different physical parameters of the tube such as length, wall thickness and inner diameter.

Effect of tube wall thickness

In order to investigate the effect of wall thickness, a series of PPy tubes was prepared as shown in Fig. 1b–g. These tubes exhibit an identical inner diameter of 1 mm, but different wall thicknesses of 45, 70 and 100 μm, corresponding to 30, 60 and 90 min of electropolymerization, respectively. At a fixed polarization potential, a maximum swelling was observed at the δ^- extremity during the first cycle of bipolar polarization, revealed by measuring the relative cross-sectional area change of the polymer tube. The degree of swelling is the highest for tubes with a thin wall and decreases with increasing wall thickness for a given electric field value and polarization time (5 V cm^{-1} for 5 s).

Furthermore, the polymer tube with the thinnest wall (synthesized in 30 min) has the shortest response time for complete swelling. The actuation depends on the charging of

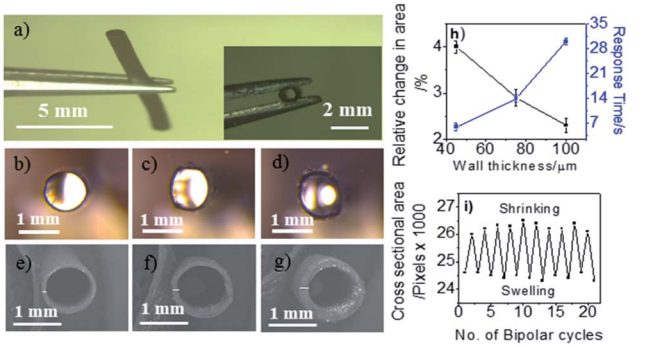

Fig. 1 Microscopic characterization and effect of wall thickness on pumping efficiency. (a) Optical picture of an as-synthesized polypyrrole tube with axial and cross-sectional (inset) views. Cross-section of the tubes recorded by optical and scanning electron microscopy (SEM) for (b and e) 45, (c and f) 75 and (d and g) 100 μm wall thickness, respectively. (h) Actuation strain expressed as the relative change in cross-sectional area (relative change of the number of pixels indicated in percent) and response time *vs.* wall thickness. (i) 10 consecutive actuation cycles for a tube with 45 μm wall thickness. Bipolar pumping was achieved by applying an electric field of 5 V cm^{-1} in 0.5 M $LiClO_4$. The tube length is 1.1 cm.

© 2021 The Author(s). Published by the Royal Society of Chemistry

Open Access Article. Published on 15 December 2020. Downloaded on 5/26/2026 11:38:55 AM.
This article is licensed under a Creative Commons Attribution-NonCommercial 3.0 Unported Licence.

the film accompanied by ion uptake or release.[52] A thick PPy tube cannot get fully charged within such a short period of time and at a low electric field. Therefore, the change in cross-sectional area or swelling effect is less pronounced.[53] A tube with thinner walls also needs less restoring force in comparison with a thicker tube and thus has a significantly shorter response time (Fig. 1h). Tubes with 45 μm walls are mechanically robust enough and were found to be more efficient in comparison with thicker tubes in terms of degree of swelling and response time. Thus, this type of tube has been chosen for further comparative studies. Practically, a polymerization time shorter than 30 min leads to tubes with insufficient mechanical strength to withstand actuation strain. Most interestingly, the tubes show reversible actuation for multiple cycles (Fig. 1i) (ESI Video S1†).

Effect of tube length

In bipolar electrochemistry experiments, a conducting object gets polarized asymmetrically along its length when exposed to the electric field. This is due to the ohmic drop in the solution leading to a gradient of electrolyte potential.[38,43] Therefore, the length of the object affects the degree of polarization, and thus also the rate of both electrochemical reactions occurring at its extremities. The kinetics of these redox reactions inducing PPy reduction and oxidation is highest at the extremities, and decreases towards the center. Therefore, it is crucial to investigate the impact of tube length on the cross-sectional area change, which greatly affects the pumping efficiency. According to the principles of bipolar electrochemistry, a longer conducting object undergoes a more pronounced polarization and thus develops higher driving forces at the extremities in comparison to shorter objects exposed to the same electric field and electrolyte medium. Consequently, longer tubes should show higher swelling and shrinking effects than shorter tubes. Here, we investigate tubes of different lengths (0.8, 1.1 and 1.5 cm), while keeping the inner diameter and the wall thickness constant (1 mm and 45 μm, respectively). It was found that longer tubes show a lower level of actuation than the shorter ones, as illustrated in Fig. 2a. This effect of the tube length on the cross sectional area change during swelling and shrinking is at first sight counter intuitive and not in agreement with the classic rules of bipolar electrochemistry. However, this can be explained by the fact that, despite their stronger polarization at the extremities, long tubes have also a long electrochemically inactive region (centre part of the tube) which represents a passive section for the propagation of pressure inside the tube, and therefore slows down the liquid flow (Fig. 2b).

In comparison, fluid pressure propagation is more efficient in a short tube, due to an only short inactive region for a given change in cross sectional area (Fig. 2c and d). However, short tubes (0.8 cm) are mechanically unstable, showing cracks after a few bipolar cycles. Even shorter tubes (below 0.8 cm) require higher electric fields to achieve the same pumping efficiency.

Effect of the inner tube diameter

In order to benefit from the law of energy conservation related to the Bernoulli principle,[54] tubes of identical wall thickness, but with variable inner diameters (600, 1000 and 1400 μm) were synthesized by using different template wires. During bipolar pumping, tubes with a smaller inner diameter undergo a more pronounced change in cross-sectional area compared to those with a bigger diameter as shown in Fig. 3. Therefore, better pumping efficiency is in principle expected for smaller diameters. Tubes with small inner diameters generate a larger force and thus a higher fluid velocity. However, too narrow tubes (600 μm) may show twisting in shape during bipolar pumping due to their larger aspect ratio. After optimizing the different parameters in terms of maximization of cross-sectional area change, a prototype of a bipolar pump was tested by optical visualization of dye release when imposing an alternating electric field. A tube with 45 μm wall thickness, 1.1 cm length and 1 mm inner diameter has been selected for these proof-of-principle pumping experiments.

Dye release as proof-of-principle for pumping

As solvent capture and release is well known to be an effect of applied potential and surface modification in the case of

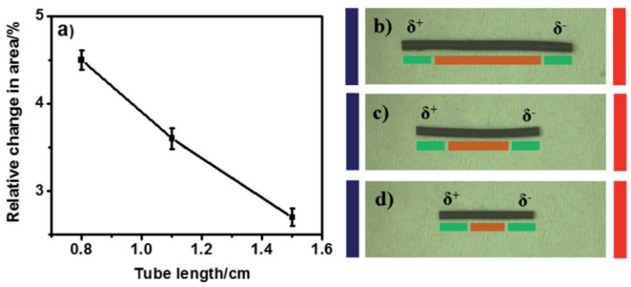

Fig. 2 (a) Relative maximum cross-sectional area change as a function of tube length in 0.5 M $LiClO_4$. (b–d) Optical images of tubes with different length (1.5, 1.1 and 0.8 cm). The orange marks indicate the electrochemically inactive part of the tube, whereas the green sections actively participate in the redox processes. The electric field is in all cases 5 V cm^{-1}. δ^+ and δ^- indicate the polarization of the PPy tube at the two extremities, red symbolizes the positive feeder electrode, blue the negative one.

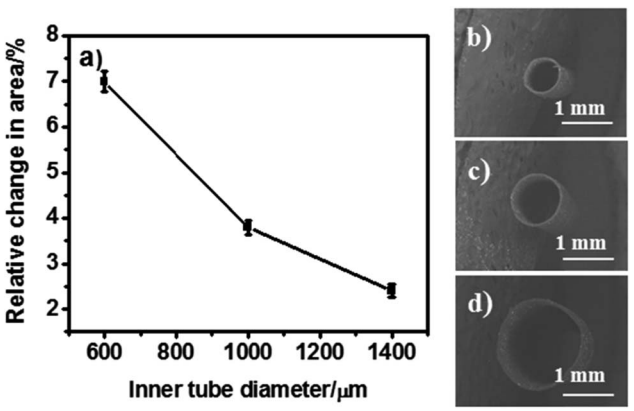

Fig. 3 (a) Relative maximum cross-sectional area change as a function of the inner tube diameter in 0.5 M $LiClO_4$. SEM images of tubes with different inner diameters (b) 600 μm (c) 1000 μm and (d) 1400 μm.

© 2021 The Author(s). Published by the Royal Society of Chemistry

Open Access Article. Published on 15 December 2020. Downloaded on 5/26/2026 11:38:55 AM.
This article is licensed under a Creative Commons Attribution-NonCommercial 3.0 Unported Licence.

PPy,[55,56] we tried to use the optimized tube structure for setting-up a prototype pumping device with an easy read-out of the hydrodynamic effects. For the dye release experiments, uni- and bi-directional dye pumping can be selectively induced on purpose, depending on the degree of asymmetry between the two tube extremities in terms of reversibility of the associated electrochemical reactions. Brilliant blue (E133) has been selected as a dye, because it has a rather low electrophoretic mobility and therefore the applied electric field does not generate a significant electrostatic migration. The dye is mixed with agarose gel, in order to slow down or prevent spontaneous release by diffusion, and then filled inside the tube. Applying an alternating electric field between the feeder electrodes leads to a release of the dye from the tube. Most interestingly, the dye release can be controlled to occur either in a symmetric/bi-directional or asymmetric/uni-directional manner. For symmetric dye release, the tube needs to be symmetric in terms of the reversibility of the electrochemical reactions occurring at both extremities. In contrast, uni-directional dye release can be achieved when the reversibility of the electrochemical reactions is not the same at both extremities. Since the as-synthesized polymer tube is initially in a fully oxidized state due to the oxidative polymerization mechanism, the level of asymmetry can be adjusted by tuning the polarization time and electric field during the very first cycle. Rapidly switching the polarity (5 s) of the feeder electrodes during the first polarization cycle at 5 V cm^{-1}, allows both extremities to undergo equivalent electrochemical transformations during subsequent cycles. This leads to an almost identical dye release from both tube ends, as shown in Fig. 4A(b–f) (ESI Video S2†).

For asymmetric or uni-directional release, the tube symmetry needs to be broken in terms of reversibility of the electrochemical reactions occurring at the two extremities. In order to break the symmetry, the first polarization cycle has to last for 25 s at a higher electric field of 6 V cm^{-1}. This condition induces a higher degree of asymmetry due to irreversible over-oxidation of one end of the tube. As a consequence, a certain fraction of the positively polarized tube end is getting over-oxidized (white patch in Fig. 4B) and therefore is not able to further participate in the redox chemistry of the polymer in subsequent cycles. This causes a stronger pumping effect, resulting in uni-directional dye release as shown in Fig. 4B(b–f) (ESI Video S3†). The pumping pressure in the case of the uni-directional dye release is stronger compared to the bi-directional release experiment, which eventually even allows pushing the agarose gel out of the tube (Fig. 4B(f)).

Expulsion of a glass sphere

After validating the uni-directional pumping of a dye, it might be of interest for some applications to further increase the pumping pressure in order to complete tasks for which stronger forces are necessary. The expulsion of a glass sphere, deliberately positioned at one outlet of the tube, was chosen for this

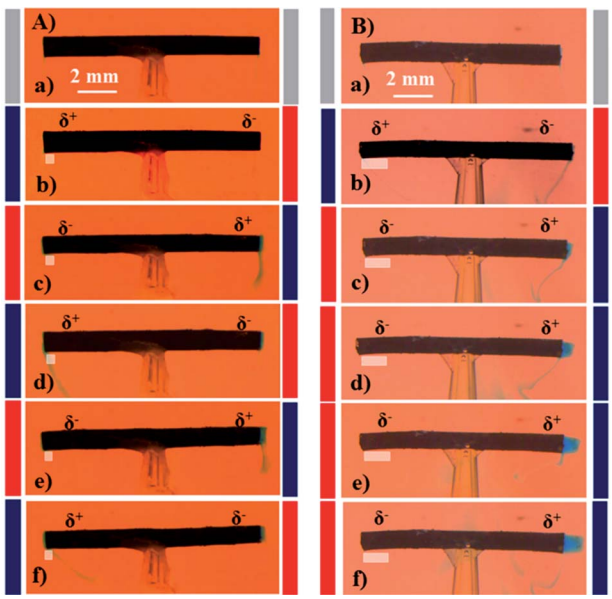

Fig. 4 Proof-of-principle for pumping with dye release. Wireless electropumping of Brilliant blue (E133) dye in 0.5 M $LiClO_4$. Red: positive feeder electrode; blue: negative feeder electrode; gray: no potential is applied at the feeder electrodes. The tube length is 1.1 cm. (A) Bi-directional pumping (a) before and (b–f) during successive bi-directional bipolar pumping cycles, (b) 1st (c) 2nd (d) 3rd (e) 4th and (f) 5th cycle with an electric field of 5 V cm^{-1}. (B) Uni-directional pumping (a) before and (b–f) during successive uni-directional bipolar pumping cycles (b) 1st (c) 4th (d) 8th (e) 12th and (f) 16th cycle with an electric field of 6 V cm^{-1}. The white patch symbolizes the over-oxidized part of the tube.

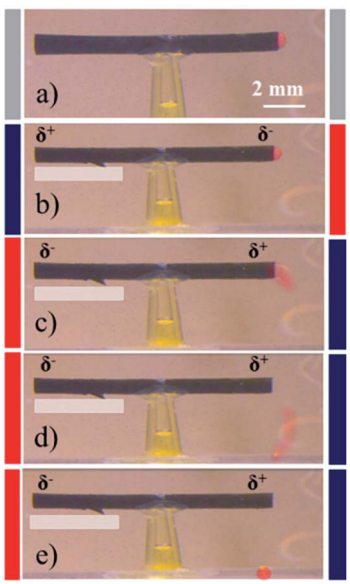

Fig. 5 Expulsion of a glass sphere. Bipolar wireless pumping allows the expulsion of a glass sphere that is located inside one extremity of the tube. Experiment performed in 0.5 M $LiClO_4$. The electric field is 10 V cm^{-1}, the tube length is 1.1 cm, with a wall thickness of 45 μm and an inner diameter of 1000 μm. (a) Before applying the electric field (b) 1st cycle of polarization and (b–e) video frames showing the position of the glass sphere during the 12 polarization cycles. The white patch indicates the over-oxidized region of the tube. The glass sphere has been artificially colored in order to enhance the contrast and ensure a better visibility.

© 2021 The Author(s). Published by the Royal Society of Chemistry

Open Access Article. Published on 15 December 2020. Downloaded on 5/26/2026 11:38:55 AM. This article is licensed under a Creative Commons Attribution-NonCommercial 3.0 Unported Licence.

purpose. In the previous experiments, electric field values of 5 and 6 V cm^{-1} were used. In order to further enhance the pumping pressure, we increased it to 10 V cm^{-1}, which is the upper limit of electric field. Above this value, the polymer becomes unstable and water electrolysis might occur at the two extremities. However, such a polarization is strong enough to develop forces and pressures even allowing the expulsion of a glass sphere located at the entrance of the tube, as an ultimate illustration of the efficiency of directional pumping. As shown in Fig. 5a–e (ESI Video S4†), after 6 polarization cycles, a sufficient force is generated by the tube to eject a rather heavy glass sphere.

Conclusion and outlook

In summary, this study describes the first set of proof-of-principle experiments, demonstrating that bipolar electrochemistry allows pumping in a tubular conducting polymer with an electric field stimulus in a straightforward and efficient way. Such wireless chemical pumping devices based on soft stimuli-responsive materials are free of several drawbacks that exist in conventional rigid pumping systems, which often require complex tools and maintenance, and, most importantly, a physical connection to a power supply. As a consequence, the concept might open up very interesting perspectives for example in the frame of a biomimetic development of polymer-based pumps for implementation in more complex fluid handling circuits. Further miniaturization might be easily achieved by using template wires with smaller diameters, which could be etched away chemically after the electropolymerization, instead of the mechanical removal used in the present work. Finally, we anticipate the possibility to design a new generation of conducting polymer based soft machines, performing in a wireless way sophisticated robotic tasks such as grasping, squeezing and stretching, which would not be possible with classic wired active elements.

Author contributions

Bh. G. and L. Z. designed and performed the experiments, wrote and edited the manuscript. A. A. M. and L. B. helped with the experimental set-up and the writing of the manuscript. B. G. helped with the design of the experimental set-up. A. K. proposed the research project, provided resources, designed experiments and edited the manuscript.

Conflicts of interest

There are no conflicts to declare.

Acknowledgements

The work has been funded by the European Research Council (ERC) under the European Union's Horizon 2020 research and innovation program (grant agreement no. 741251, ERC Advanced grant ELECTRA). This study has also received financial support from the French State in the framework of the "Investments for the future" Program, IdEx Bordeaux, reference ANR-10-IDEX-03-02. L. Z. acknowledges financial support from the National Natural Science Foundation of China (No. 21902045).

References

1 C. Li, S. Feng, C. Li, Y. Sui, J. Shen, C. Huang, Y. Wu and W. Huang, *Adv. Funct. Mater.*, 2020, 2002163.
2 A. K. Mishra, T. J. Wallin, W. Pan, P. Xu, K. Wang, E. P. Giannelis, B. Mazzolai and R. F. Shepherd, *Sci. Robot.*, 2020, **5**, eaaz3918.
3 R. Lan, J. Sun, C. Shen, R. Huang, Z. Zhang, C. Ma, J. Bao, L. Zhang, L. Wang, D. Yang and H. Yang, *Adv. Funct. Mater.*, 2020, 2000252.
4 V. Cacucciolo, J. Shintake, Y. Kuwajima, S. Maeda, D. Floreano and H. Shea, *Nature*, 2019, **572**, 516–519.
5 X. Liu, J. Liu, S. Lin and X. Zhao, *Mater. Today*, 2020, **36**, 102–124.
6 Q. Chen, Y. Li, Y. Yang, Y. Xu, X. Qian, Y. Wei and Y. Ji, *Chem. Sci.*, 2019, **10**, 3025–3030.
7 F. Mushtaq, H. Torlakcik, M. Hoop, B. Jang, F. Carlson, T. Grunow, N. Läubli, A. Ferreira, X. Z. Chen, B. J. Nelson and S. Pané, *Adv. Funct. Mater.*, 2019, 1808135.
8 L. Chen, M. Weng, P. Zhou, F. Huang, C. Liu, S. Fan and W. Zhang, *Adv. Funct. Mater.*, 2019, **29**, 1806057.
9 X. Wang, B. Yang, D. Tan, Q. Li, B. Song, Z. S. Wu, A. del Campo, M. Kappl, Z. Wang, S. N. Gorb, S. Liu and L. Xue, *Mater. Today*, 2020, **35**, 42–49.
10 Q. Chen, X. Yu, Z. Pei, Y. Yang, Y. Wei and Y. Ji, *Chem. Sci.*, 2016, **8**, 724–733.
11 M. Loepfe, C. M. Schumacher, C. H. Burri and W. J. Stark, *Adv. Funct. Mater.*, 2015, **25**, 2129–2137.
12 Y. Cheng, K. H. Chan, X. Q. Wang, T. Ding, T. Li, X. Lu and G. W. Ho, *ACS Nano*, 2019, **13**, 13176–13184.
13 H. Lin, S. Ma, B. Yu, M. Cai, Z. Zheng, F. Zhou and W. Liu, *Chem. Mater.*, 2019, **31**, 4469–4478.
14 L. Ionov, *Mater. Today*, 2014, **17**, 494–503.
15 M. Mohammed, P. Thurgood, C. Gilliam, N. Nguyen, E. Pirogova, K. Peter, K. Khoshmanesh and S. Baratchi, *Anal. Chem.*, 2019, **91**, 12077–12084.
16 B. Yan, B. Li, F. Kunecke, Z. Gu and L. Guo, *ACS Appl. Mater. Interfaces*, 2015, **7**, 14563–14568.
17 Y. Shiraki and R. Yoshida, *Angew. Chem., Int. Ed.*, 2012, **51**, 6112–6116.
18 J. A. Lv, Y. Liu, J. Wei, E. Chen, L. Qin and Y. Yu, *Nature*, 2016, **537**, 179–184.
19 J. S. Moore, J. M. Bauer, Q. Yu, R. H. Liu, C. Devadoss and B. Jo, *Nature*, 2000, **404**, 588–590.
20 S. Babu, P. Ndungu, J.-C. Bradley, M. P. Rossi and Y. Gogotsi, *Microfluid. Nanofluid.*, 2005, **1**, 284–288.
21 S. Ramírez-García and D. Diamond, *Sens. Actuators, A*, 2007, **135**, 229–235.
22 Y. Wu, D. Zhou, G. M. Spinks, P. C. Innis, W. M. Megill and G. G. Wallace, *Smart Mater. Struct.*, 2005, **14**, 1511–1516.
23 T. F. Otero, J. J. Sanchez and J. G. Martinez, *J. Phys. Chem. B*, 2012, **116**, 5279–5290.

© 2021 The Author(s). Published by the Royal Society of Chemistry

Open Access Article. Published on 15 December 2020. Downloaded on 5/26/2026 11:38:55 AM. This article is licensed under a Creative Commons Attribution-NonCommercial 3.0 Unported Licence.

24 L. V. Conzuelo, J. Arias-Pardilla, J. V. Cauich-Rodríguez, M. A. Smit and T. F. Otero, *Sensors*, 2010, **10**, 2638–2674.
25 J. Shklovsky, A. Reuveny, Y. Sverdlov, S. Krylov and Y. Shacham-Diamand, *Microelectron. Eng.*, 2018, **199**, 58–62.
26 B. Gupta, B. Goudeau, P. Garrigue and A. Kuhn, *Adv. Funct. Mater.*, 2017, 1705825.
27 J. Tangorra, P. Anquetil, T. Fofonoff, A. Chen, M. Del Zio and I. Hunter, *Bioinspiration Biomimetics*, 2007, **2**, S6–S17.
28 J. G. Martinez and T. F. Otero, *J. Phys. Chem. B*, 2012, **116**, 9223–9230.
29 F. García-Córdova, L. Valero, Y. A. Ismail and T. F. Otero, *J. Mater. Chem.*, 2011, **21**, 17265–17272.
30 F. Mashayekhi Mazar, J. G. Martinez, M. Tyagi, M. Alijanianzadeh, A. P. F. Turner and E. W. H. Jager, *Adv. Mater.*, 2019, **31**, 1901677.
31 S. Y. Yang, S. K. Mahadeva and J. Kim, *Smart Mater. Struct.*, 2010, **19**, 105026.
32 B. Gupta, B. Goudeau and A. Kuhn, *Angew. Chem., Int. Ed.*, 2017, **56**, 14183–14186.
33 L. Zhang, B. Gupta, B. Goudeau, N. Mano and A. Kuhn, *J. Am. Chem. Soc.*, 2018, **140**, 15501–15506.
34 S. Assavapanumat, B. Gupta, G. Salinas, B. Goudeau, C. Wattanakit and A. Kuhn, *Chem. Commun.*, 2019, **55**, 10956–10959.
35 S. Arnaboldi, B. Gupta, T. Benincori, G. Bonetti, R. Cirilli and A. Kuhn, *Anal. Chem.*, 2020, **92**, 10042–10047.
36 L. Koefoed, S. U. Pedersen and K. Daasbjerg, *Curr. Opin. Electrochem.*, 2017, **2**, 13–17.
37 Z. A. Fattah, L. Bouffier and A. Kuhn, *Appl. Mater. Today*, 2017, **9**, 259–265.
38 S. E. Fosdick, K. N. Knust, K. Scida and R. M. Crooks, *Angew. Chem., Int. Ed.*, 2013, **52**, 10438–10456.
39 S. Tiewcharoen, C. Warakulwit, V. Lapeyre, P. Garrigue, L. Fourier, C. Elissalde, S. Buffière, P. Legros, M. Gayot, J. Limtrakul and A. Kuhn, *Angew. Chem., Int. Ed.*, 2017, **56**, 11431–11435.
40 N. Shida, Y. Zhou and S. Inagi, *Acc. Chem. Res.*, 2019, **52**, 2598–2608.
41 Y. Ishiguro, S. Inagi and T. Fuchigami, *J. Am. Chem. Soc.*, 2012, **134**, 4034–4036.
42 S. Inagi, Y. Ishiguro, M. Atobe and T. Fuchigami, *Angew. Chem., Int. Ed.*, 2010, **49**, 10136–10139.
43 G. Loget, D. Zigah, L. Bouffier, N. Sojic and A. Kuhn, *Acc. Chem. Res.*, 2013, **46**, 2513–2523.
44 W. F. Paxton, S. Sundararajan, T. E. Mallouk and A. Sen, *Angew. Chem., Int. Ed.*, 2006, **45**, 5420–5429.
45 F. Mavré, R. K. Anand, D. R. Laws, K. F. Chow, B. Y. Chang, J. A. Crooks and R. M. Crooks, *Anal. Chem.*, 2010, **82**, 8766–8774.
46 A. De Poulpiquet, B. Diez-Buitrago, M. Dumont Milutinovic, M. Sentic, S. Arbault, L. Bouffier, A. Kuhn and N. Sojic, *Anal. Chem.*, 2016, **88**, 6585–6592.
47 A. Ismail, S. Voci, P. Pham, L. Leroy, A. Maziz, L. Descamps, A. Kuhn, P. Mailley, T. Livache, A. Buhot, T. Leichlé, A. Bouchet-Spinelli and N. Sojic, *Anal. Chem.*, 2019, **91**, 8900–8907.
48 F. AlTal and J. Gao, *J. Am. Chem. Soc.*, 2018, **140**, 9737–9742.
49 B. Gupta, M. C. Afonso, L. Zhang, C. Ayela, P. Garrigue, B. Goudeau and A. Kuhn, *ChemPhysChem*, 2019, **20**, 941–945.
50 R. Kiefer, J. G. Martinez, A. Kesküla, G. Anbarjafari, A. Aabloo and T. F. Otero, *Sens. Actuators, B*, 2016, **233**, 328–336.
51 M. J. M. Jafeen, M. A. Careem and S. Skaarup, *Ionics*, 2010, **16**, 1–6.
52 W. Zheng, P. G. Whitten and G. M. Spinks, *Multifunct. Mater.*, 2018, **1**, 014002.
53 Z. Li, Y. Seo, O. Aydin, M. Elhebeary, R. D. Kamm, H. Kong and M. A. Taher Saif, *Proc. Natl. Acad. Sci. U. S. A.*, 2019, **116**, 1543–1548.
54 M. Widden, Fluid Dynamics: Continuity Principle and Bernoulli's equation, in *Fluid Mechanics*, ed. G. E. Drabble, Palgrave, London, Foundations of Engineering Series, 1996, pp. 151–200.
55 W. Xu, A. Palumbo, J. Xu, Y. Jiang, C. H. Choi and E. H. Yang, *ACS Appl. Mater. Interfaces*, 2017, **9**, 23119–23127.
56 G. Chatzipirpiridis, A. Sanoria, O. Ergeneman, J. Sort, J. Puigmartí-Luis, B. J. Nelson, E. Pellicer and S. Pané, *Electrochem. Commun.*, 2015, **54**, 32–35.

© 2021 The Author(s). Published by the Royal Society of Chemistry